Al-Qadisiyah Journal for Engineering Sciences 17 (2024) 445–456

Contents lists available at http://qu.edu.iq

Al-Qadisiyah Journal for Engineering Sciences

Journal homepage: https://qjes.qu.edu.iq

Dynamic simulation of solar-powered desalination with integrated photovoltaic/thermal collectors and membrane distillation

Ahmed Remlaoui [1]*, Driss Nehari [1], Benhanifia Kada [2], Hitesh Panchal [3], Khaled Al-Farhany [4] and Mohamed Al-Dawody [4]

[1]*Applied Hydrology and Environment Laboratory, University of Ain Témouchent - BELHADJ Bouchaib, 46000 Ain-Témouchent, Algeria*
[2] *Laboratory of Energy in Arid Region (ENERGARID), Faculty of Science and Technology, University of Tahri Mohamed Bechar, Bechar 08000, Algeria*
[3]*Mechanical Engineering Department, Government Engineering College Patan, Gujarat, India*
[4]*Department of Mechanical Engineering, University of Al-Qadisiyah, Ad-Diwaniyah, 58001, Iraq*

ARTICLE INFO

Article history:
Received 01 June 2024
Received in revised form 10 October 2024
Accepted 10 December 2024

Keywords:
Solar desalination
Photovoltaic/thermal collector
Direct contact membrane distillation dynamic
Simulation
TRNSYS
Distillate production

ABSTRACT

This study describes a computational model that simulates the behaviour of a solar-powered desalination system. The model incorporates photovoltaic/thermal (PVT) collectors and direct contact membrane distillation (DCMD). A novel DCMD unit model was established and verified using existing data from the literature, and the model was incorporated into the TRNSYS library. The effect of feed water mass flow rate and temperature on production was investigated through a parametric analysis. The PVT-DCMD system was modelled, analysed, and dynamically simulated for the month of June in Algeria using TRNSYS software. Results show that the PVT collector's outlet solar fluid temperature ranges from 20 °C to 85 °C, providing 5000 kJ/hr of useful energy for seawater desalination through a heat exchanger. Meanwhile, the auxiliary heater utilises around 10,000 kJ/hr of solar energy. The simulation demonstrates the feasibility and effectiveness of using PVT collectors with a DCMD system for seawater desalination, achieving a distillate production rate of approximately 12 L/hr.m^2 of membrane.

1. Introduction

In response to the increasing demand for freshwater, desalination stations have become critical infrastructure in Algeria, Iraq, and other Arab countries. These facilities are vital in converting seawater into potable water, effectively addressing water scarcity challenges in arid regions. Similarly, other Arab nations grappling with similar water scarcity issues have significantly invested in desalination projects. For instance, Yemen, particularly in cities like Taiz [1], has recognised desalination technology's importance in securing a sustainable water supply for its population. In recent years, there has been a notable surge in the demand for freshwater in developing nations, including Algeria, resulting in a corresponding rise in the establishment of desalination facilities. These facilities use much electricity, predominantly sourced from non-renewable energy resources such as natural gas, petroleum, coal, and nuclear power. The widespread utilisation of these energy sources contributes to their gradual exhaustion, resulting in an escalation of energy prices and environmental concerns. Hence, the need for sustainable energy sources has gained increasing interest. Renewable energies, such as solar energy, are considered promising for addressing these difficulties. Solar energy is abundant in Algeria, making it a logical source for salt-water desalination methods like membrane desalination.

* *Corresponding author.*
E-mail address: *ahmed.remlaoui@univ-temouchent.edu.dz* (Ahmed Remlaoui)

https://doi.org/10.30772/qjes.2024.151057.1275

Nomenclature:

A	Membrane area, m^2
A_{PVT}	PVT collector surface area, m^2
C_{global}	Membrane mass transfer coefficient, L/(m^2h.Pa)
C_p	Specific heat capacity, kJ.$kg^{-1}K^{-1}$
E	Electric energy rate output, W
G_t	Total tilted surface radiation for surface, W/m^2
ΔH_v	Latent heat of water vaporisation, J L^{-1}
J_w	Mass flux, L/(m^2.hr)
$\dot{m}$	Mass flow rate, Kg/hr
P	Partial pressures, Pa
Q	Energy rate, W
T	Temperature, °C
Ta	Ambient temperature, °C
Tp	PVT panel temperature, °C
ΔT	Temperature change, °C
U	Transfer coefficient, J.$hr^{-1}m^{-2}K^{-1}$
U_l	Total heat loss coefficient, W/m^2K
V	Stream velocity,m/s
W	Membrane width, m

Greek symbols

f	Pump power fraction of the heat converted to solar fluid.
γ	Control signal
η_0	Optical solar collector performance of the PVT, %
η_e	Photovoltaic efficiency, %
η_{th}	Thermal efficiency, %
f	Pump power fraction of the heat converted to solar fluid.
γ	Control signal

Subscripts

bf	Feed side at membrane surface position.
bp	Permeate side at membrane surface position.
h	Upper.
high limit	High-limit condition.
in	Inlet
l	Lower.
out	Outlet
rated	Rated flow rate
sf	Solar fluid

Files must be in MS Word only and should be formatted for direct printing. Membrane distillation (MD) is a thermal/membrane hybrid technology that has demonstrated significant promise in the production of desalinated water with high recovery rates (>90%) and low energy consumption.

The process of membrane distillation (MD) entails the utilisation of a microporous hydrophobic membrane, which is in direct contact with a heated solution on the feed side. The membrane's impermeability is attributed to its hydrophobic properties, which effectively hinder the passage of any liquid substance. However, it still allows for the presence of a vapour-liquid interface at the entrance of each pore. During the process, water evaporates while non-volatile solutes remain in the solution. The water vapour then diffuses across the membrane and subsequently condenses on the opposite side of the module, ultimately leading to the production of distilled water. In theory, this procedure ensures the total exclusion of non-volatile solutes, including macromolecules, colloidal species, and ions. Typically, temperature differences ranging from 50 to 80 °C are deemed sufficient for achieving a desirable transmembrane flow rate of 1-10 L/m^2h. This facilitates the effective utilisation of sustainable energy resources that provide moderate temperature heat [2]. MD achieves exceptional rejection rates for ions and non-volatile solutes, reaching up to 99.9%. This superior rejection capability ensures enhanced water purity compared to Reverse Osmosis (RO). Additionally, MD operates at atmospheric pressure. In contrast, RO can integrate with wind turbines to provide Maximum Power Point and Maximum Permeate Flow Tracking [3]. Among the four MD systems identified in the literature [4-6], these studies review the four membrane distillation configurations: Direct Contact Membrane Distillation (DCMD), Air Gap Membrane Distillation (AGMD), Vacuum Membrane Distillation (VMD), and Sweep Gas Membrane Distillation (SGMD). Direct Contact Membrane Distillation is commonly regarded as the most extensively studied arrangement, mainly owing to its straightforward setup and relatively high flux rate compared to alternative configurations [6].

Several experimental and numerical studies have been carried out over the years on solar membrane distillation (MD) desalination systems. Remlaoui et al. [6] developed a TRNSYS model for simulating a water desalination system employing direct contact membrane distillation (DCMD) powered by flat plate solar collectors (FPCs) [6]. The study's findings indicate that the desalination system can generate a daily distillate output of approximately 42.86 L/day. Furthermore, the specific daily distillate production rate is determined to be 10.85 kg/m^2 of flat plate collector (FPC) area. TRNSYS 17 is a robust simulation platform that offers extensive capabilities for conducting transient system simulations [7]. Kumar and Martin [8] undertook a series of tests and simulations to examine the integration of membrane distillation with solar household heaters (SCMD) to produce domestic heat and pure water simultaneously. The researchers evaluated many strategies and determined the most effective ones for practical use. The research on the integrated solar system successfully achieved the simultaneous production of 20 L/day of potable water and 250 L/day of heated water, without additional heating mechanisms, to fulfil the requirements of a single residential unit. The SCMD system's validity was assessed by employing a TRNSYS simulation model. This model replicated the Air Gap Membrane Distillation using empirical laboratory data. The simulation results indicated that the SCMD system has the capability to function at an efficiency of 80%. In a separate investigation, Mohan et al. [9] conducted a numerical simulation and analysis of an innovative solar thermal poly generation system that incorporates membrane distillation alongside three distinct types of solar collectors: flat plate collectors (FPCs), evacuated tube collectors (ETCs), and compound parabolic collectors (CPCs). The economic study undertaken for the three collector configurations revealed that the Evacuated Tube Collector (ETC) exhibited the shortest payback period, at 9 years. In addition, Achmad et al. [10] devised a comprehensive desalination system powered by solar energy. This system integrates solar photovoltaic (PV) and solar thermal collectors with a Memsys Vacuum Multi-Effect Membrane Distillation (V-MEMD) module. The objective of this system was to attain autonomous functionality in arid and remote regions of Saudi Arabia. The findings revealed that the average conductivity of the distilled water generated by the system was 6.2 µs/cm, while the most favourable feed flow rate was 69 L/h. Relatedly, innovative photovoltaic/thermal (PVT) solar technologies have been introduced separately for PV or thermal applications. These panels incorporate both solar photovoltaic (PV) modules and solar thermal collectors, allowing them to generate electricity from solar radiation and simultaneously recover heat through a working fluid. This is achieved by utilising both photovoltaic and thermal recovery systems in PVT panels [11]. In the present context, the PVT collector [12] was examined and simulated across various applications and utilising multiple software applications [13-18]. For instance, the utilisation of solar residential hot water systems has been extensively studied [19-23]. The implementation of solar heating and cooling systems has also been explored [24, 25]. In prior research on solar multi-effect distillation (MD) systems, it was found that flat plate collectors (FPC) and evacuated tube collectors (ETC) were widely recognised for their effectiveness in desalination processes. Furthermore,

these systems were often integrated with either grid-connected electricity or a separate photovoltaic (PV) system, which operated independently from the thermal system. The cost of individual systems is usually higher than the combined photovoltaic-thermal (PVT) system. The PVT collector has undergone thorough examination and simulation across various study domains, utilising different software packages [13-18]. The PVT collector has been utilised in solar household hot water systems [19-23] as well as solar heating and cooling systems [24, 25]. Previous research on solar membrane distillation (MD) systems has consistently advocated for the use of both flat plate collectors (FPC) and evacuated tube collectors (ETC) for desalination applications. These collectors can be integrated with the electrical grid or operated independently through a dedicated photovoltaic (PV) system. Nevertheless, the standalone photovoltaic (PV) system incurs higher costs compared to the integrated photovoltaic-thermal (PVT) system.

Although there is considerable interest in the integration of photovoltaic-thermal (PVT) systems with membrane distillation (MD) for solar desalination, the number of studies undertaken on this topic thus far is limited [26, 27, 29-32]. One of the investigations conducted by Acevedo et al. [26] entailed the modelling and analysis of a compact pilot facility that produces energy, domestic hot water (DHW), and fresh water (FW). The system comprises of photovoltaic/thermal (PVT) collectors, a wind turbine (WT), evacuated tube collectors (ETCs), Permeate Gap Membrane Distillation (PGMD), and reverse osmosis (RO) for the production of solar hot water (SHW) and fresh water (FW). The findings demonstrated that the system under consideration successfully generated a maximum annual output of 15.311 litres of fresh water and 1.890 kwh of electrical energy.

The merging of AGMD with concentrated photovoltaic thermal (CPVT) systems for seawater desalination was proposed by Hughes et al. [27]. Based on their findings, the utilisation of a 1 m^2 CPVT aperture area yields 3.4 L/h of fresh water [28]. The patent by Davis and Cappelle [29] also provided confirmation of the integration of PVT and MD. Furthermore, in a study conducted by Andrew et al. [30], the authors empirically integrated the CPVT and DCMD systems. The system comprised a dual-ring configuration, whereby the initial ring facilitated salt-water heating using Concentrated Photovoltaic Thermal (CPVT) technology. Subsequently, the second ring facilitated the circulation of the heated saline water, which possessed a salinity level of 1%, through the Direct Contact Membrane Distillation (DCMD) module. This module incorporated a polytetrafluoroethylene membrane with a surface area of 0.0491 m^2, thereby enabling desalination. The experimental findings indicated that the permeate flux attained a value of 7.1 L/m^2h. Wiesenfarth et al. also accomplished the integration of the CPVT+MD system with reverse osmosis [32]. According to reference [28], the system possessed an aperture area measuring 15.9 m^2 and exhibited a water recovery capacity of 92 %. Despite the existing incentive to investigate solar desalination systems that integrate photovoltaic-thermal (PVT) technology and membrane distillation (MD), there is a scarcity of simulations and practical investigations conducted in this area.

Many research studies have recently been conducted to investigate the experimental, numerical, and theoretical aspects of solar-powered desalination systems. For example, Guopei Li et al. [33] report a unique investigation regarding a sweeping gas membrane distillation desalination plant intended for insular and coastal families. Using solar thermal collectors and photovoltaic arrays, this structure produces 9.98 kg to 23.26 kg of fresh water daily, more than enough to cover the needs of a typical household of four. With a thermal efficiency of 50%, the solar collector area significantly impacts system performance.

Furthermore, Zhaoli Zhang et al. [34] provide a focused photovoltaic/thermal-multiple effect distillation system designed for remote islands that simultaneously offers energy, warmth, and drinking. The study's theoretical evaluation demonstrates effective outcomes with high energic and exergetic efficiencies, demonstrating the system's superior effectiveness in overall solar energy usage. Another study [35] describes a solar hybrid desalination facility that combines photovoltaic thermal collectors with reverse osmosis desalination. This setup offers enhanced water recovery, lower power usage, and a cost-competitive supply of fresh water at \$0.719/m^3, demonstrating the potential of hybrid systems to address water concerns. In a separate study, Qian Chen et al. [36] investigate an autonomous water/electricity cogeneration plant which combines focused photovoltaic/thermal collectors with vacuum multi-effect membrane distillation. The technology transforms around 70% of solar irradiation into helpful electricity, showing excellent compactness and increased thermodynamic efficiency. The analysis gives yearly energy and water production rates per m^2 of solar collector area, shedding light on the system's economic feasibility. This research aims to examine and improve understanding of the synergistic utilisation of solar energy in the simultaneous generation of thermal energy for heating seawater and electrical energy for desalination applications. The system under consideration involves integrating the SSH (Solar Salt-water Heating) system with PVT and DCMD technologies for salt-water desalination. This integration incorporates two distinct loops within the system. The study encompasses various facets, encompassing the creation of a novel TRNSYS component for the DCMD system utilising Fortran software, exploration of the influence of feed temperature and velocity on the permeate flow, and assessment of the efficacy of the integrated PVT and DCMD process in solar-driven desalination.

2. Mathematical modelling of the DCMD system

In a prior investigation by the authors [6], a numerical model was formulated to simulate a Direct Contact Membrane Distillation (DCMD) module. The model was based on the use of a straightforward mass transfer coefficient and the overall heat transfer properties of the membrane. The model presented in this study was evaluated against experimental and modelling findings conducted by Zhang et al. [37], who employed identical membrane characteristics and hydrodynamic conditions. The mass transfer J_w (L/(m^2h)) can be determined by a linear function that combines the membrane permeability C_{global} (L/(m^2h.Pa)) and the vapour pressure difference across the membrane [37,38]. This relationship is represented by equation (1) in Table 1. The partial pressures in the feed and permeate sides, P_{bf} and P_{bp} (Pa), are functions of the temperature at the membrane surface, T_{bf} and T_{bp}, which can be calculated using the Antoine equation (Eq. (2)), as shown in Figure 1. A simple model for heat transfer in the DCMD module, which assumes that C_{global} and U are constants and presented in Eqs. (3-11). The feed and permeate temperatures at the (i+1)th station can be calculated using equations (8) and (9), and the total mass and heat flux transferred at this station are given by equations (10) and (11).

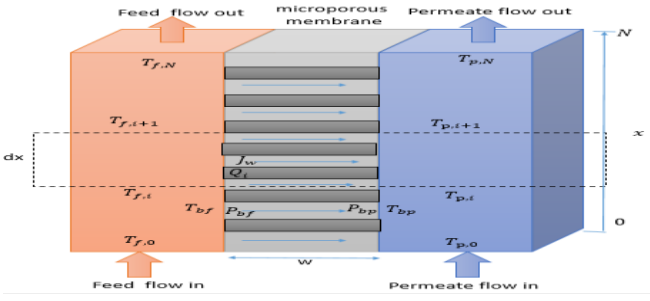

Figure 1. Schematic of DCMD module under the co-current flow mode.

Table 1. Mass and heat equations of the DCMD system

Parameter	Equation	Equation number
Mass transfer [33,34]	$J_w = C_{global}(P_{bf} - P_{bp})$	(1)
Partial pressures of water at feed and permeate sides	$P_{bf,p} = \exp\left(23.1964 - \frac{3816.44}{T_{bf,p} + 227.04}\right)$	(2)
Overall heat transfer coefficient	$U = -5248V^2 + 4735.7V - 36.036$	(3)
Mass transfer coefficient	$C_{global} = -0.004V^2 + 0.0053V - 0.0001$	(4)
Heat change in the hot side, cold side and membrane	$C_{p,f}\dot{m}_f(T_{f,i+1} - T_{f,i}) = U(T_{f,i} - T_{p,i})dA + J_w\Delta H_v dA = C_{p,p}\dot{m}_p(T_{p,i} - T_{p,i+1})$	(5)
Feed temperature change	$\Delta T_{f,i} = -\frac{[U(T_{f,i} - T_{p,i}) + J_w\Delta H_v]wdx}{C_{p,f}\,\dot{m}_{f,i}}$	(6)
Permeate temperature change	$\Delta T_{p,i} = \frac{[U(T_{f,i} - T_{p,i}) + J_w\Delta H_v]wdx}{C_{p,p}\,\dot{m}_{p,i}}$	(7)
Feed temperatures at $(i+1)^{th}$ station	$T_{f,i+1} = T_{f,i} - \Delta T_{f,i}$	(8)
Permeate temperatures at $(i+1)^{th}$ station	$T_{p,i+1} = \Delta T_{p,i} - T_{p,i}$	(9)
Mass flux at $(i+1)^{th}$ station	$J_{i+1} = C_{global}(P_{f,i+1} - P_{p,i+1})$	(10)
Heat flux at the $(i+1)^{th}$ station	$Q_{i+1} = U(T_{f,i+1} - T_{p,i+1})$	(11)

3. System description

The present study proposes a model for the production of freshwater from seawater and thermal energy. This model involves the combination of Direct Contact Membrane Distillation (DCMD) and Photovoltaic/Thermal System (PVT), as illustrated in Figure 2. The fundamental solar distillation system comprises photovoltaic/thermal (PVT) collectors, an auxiliary heater, a heat exchanger, a pump, and a direct contact membrane distillation (DCMD) module.

A battery, regulator/inverter, and PVT collectors are connected to power the auxiliary electrical heater in the storage tank and pumps. The system is designed to operate in Ain Témouchent, Algeria, during the day from 08:00 to 18:00 hours.

Meanwhile, thermal energy is delivered by a PVT, where the heat transfer fluid (HTF) captures solar energy and provides thermal energy at the same time. After that, the heated fluid is sent to a thermal storage tank. The heat from the HTF is transferred to the seawater via a coil heat exchanger.

The electrical system comprises a solar panel, a battery bank, and an independent inverter. This autonomous system utilises DC to AC conversion to provide power to the pump and supplementary heater located in the storage tank. The chemical storage of direct current electrical energy for future use is the primary function of battery packs, particularly in overcast weather conditions. During the DCMD process, a heated feed solution (salt water) is delivered to the module. A fraction of the feed solution (gas) infiltrates the membrane and combines with the cooling liquid on the permeate side. The remaining feed solution, referred to as the concentrate, exits the module through the feed side.

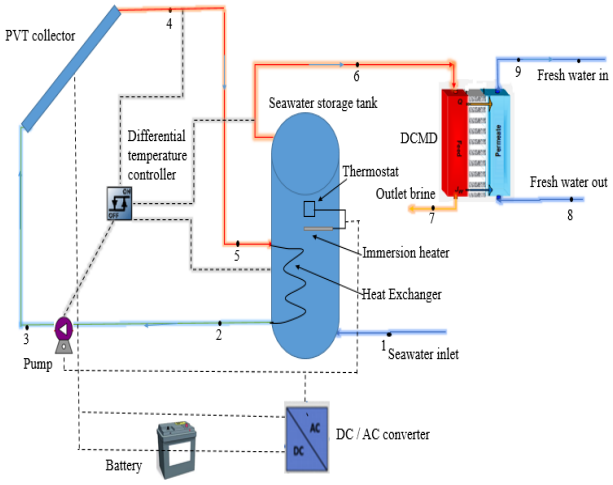

Figure 2. Schematic diagram of solar-DCMD plant.

4. TRNSYS Simulation

TRNSYS software has been employed to evaluate the performance of the proposed system, which is modelled using various component simulation models known as TRNSYS types (see Figure 3). These include Weather Data Reading and Processing (TYPE15-6TM2), Constant Speed Pump (Type 3d), Stratified Fluid Storage Tank with Internal Heat Exchangers (Type 60d), Time Dependent Forcing Function (Water supply profile) (Type 14b), Differential Temperature Controller (Type 2b), Unit Conversion Routine (Type 57), Online Plotter with File (Type 65c), PVT collector (Type 50a), Electrical Storage (Type 47c), Regulator/Inverter (Type 48b), and a newly programmed DCMD module (Type 223).

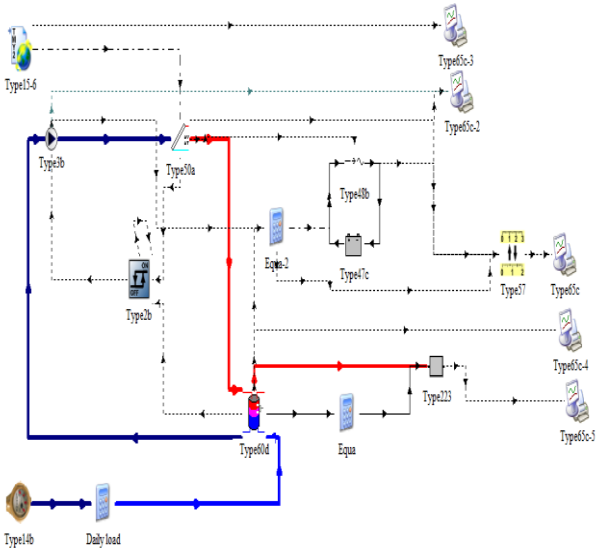

Figure 3. Solar PVT and DCMD systems modelled in TRNSYS 17.

4.1 PVT collector

In the TRNSYS model, the PVT collectors were simulated using TYPE50a and their parameters are detailed in Table 2. The Hottel-Whillier equation is used to estimate the thermal efficiency of the PVT collectors [39], taking into account the effective product between the transparent cover transmittance and the absorption $(\tau\alpha)_e$, total heat loss coefficient (U_l in

W/m²K), PVT rear panel temperature (T_p) and ambient temperature (T_a), and solar radiation (G_t in W/m²):

$$\eta_{th} = (\tau\alpha)_e - U_l\left(\frac{T_p - T_a}{G_t}\right) \quad (12)$$

The photovoltaic efficiency is calculated by dividing the electric energy output (E in W) by the solar radiation (G_t in W/m²) over the PVT area (A_{PVT} in m²) [39], using the optical performance of the PVT (η_0) and the thermal loss coefficients (C_1 and C_2):

$$\eta_e = \left(\frac{E}{A_{PVT}G_t}\right) = \eta_0 - \frac{C_1(T_p - T_a) - C_2(T_p - T_a)^2}{G_t} \quad (13)$$

Table 2. Parameters for PVT collector of Type 50a.

Parameter	Value
Area of collector (m²)	02.00
Efficiency factor of collector fin	00.96
Thermal capacitance of fluid (kJ/kg K)	3.708
Absorptance of the collector plate	00.92
Loss coefficient of the collector (kJ/h m² K)	16.00
Transmittance of cover	00.89
Coefficient of temperature impact on solar cell efficiency	0.0032
Cell efficiency referenced at a specific temperature (°C)	25.00
Factor related to packing	00.80

4.2 Seawater storage tank

The Type 60 model is a comprehensive design created explicitly for stratified fluid storage tanks, as shown in Figure 4. It incorporates the possibility of incorporating internal heat exchangers, which enhances its use for simulating commercially accessible domestic hot water tanks intended for solar applications. This model's computational intensity and robustness are comparatively lower than Type 4, mostly because of its intricate modelling method that incorporates iterative loops for heat exchanger coefficients, node energy balance, and internal heater management [7]. Table 3 contains the parameters pertaining to the seawater storage tank utilised inside the TRNSYS model.

In order to simulate the thermal behaviour of a thermally stratified energy storage tank containing water, the reservoir can be approximated as comprising N (where N < 100) uniformly sized segments that are completely mixed. This assumption allows for the modelling of the tank's thermal performance. When calculating the energy balance, it is essential to consider all energy flows in and out of a node (layer). This includes energy transfers associated with mass flow (injected flow, Q_{inject}), conduction (Q_{cond}), convection (Q_{env}), auxiliary power (Q_{aux}), and internal heat exchanger flows within the tank (flows the layers, Q_{flue}):

$$M_i C_p \frac{dT_i}{dt} = Q_{env} + Q_{cond} + Q_{hx} + Q_{aux} + Q_{inject} + Q_{flue} \quad (14)$$

Table 3. Characteristics of hot water tank (Type 60d) [40].

variable	Value
Volume of tank (m³)	0.3
Height of tank (m)	1.68
Inlet 1 height (m)	0.1
Outlet 1 height (m)	1.6
Specific heat of fluid (kJ kg^{-1} K^{-1})	3.850
Density of fluid (kg m^{-3})	1025
The coefficient for tank heat loss (W m^{-2} K^{-1})	0.3
Thermal conductivity of fluid (kJ hr^{-1} m^{-1} K^{-1})	1.4
The temperature at which boiling occurs (°C)	100
Elevation of auxiliary heater (m)	1
Elevation of thermostat (m)	1.5
Reference temperature for system element (°C)	60
Temperature range for heating element's operation (°C)	5
Peak heating rate of system element (kJ hr^{-1})	9900
Proportion of glycol in mixture.	0.4
Inside diameter of heat exchanger (m)	0.016
The outside diameter of the heat exchanger (m)	0.02
Fin diameter of heat exchanger (m)	0.02
Overall surface area of heat exchanger (m²)	2
Length of heat exchanger (m)	32
Thermal conductivity of heat exchanger wall (kJ hr^{-1} m^{-1} K^{-1})	1.8
Thermal conductivity of the material in the heat exchanger (kJ hr^{-1} m^{-1} K^{-1})	1.8
Inlet height of heat exchanger (m)	0.9
Outlet height of heat exchanger (m)	0.1

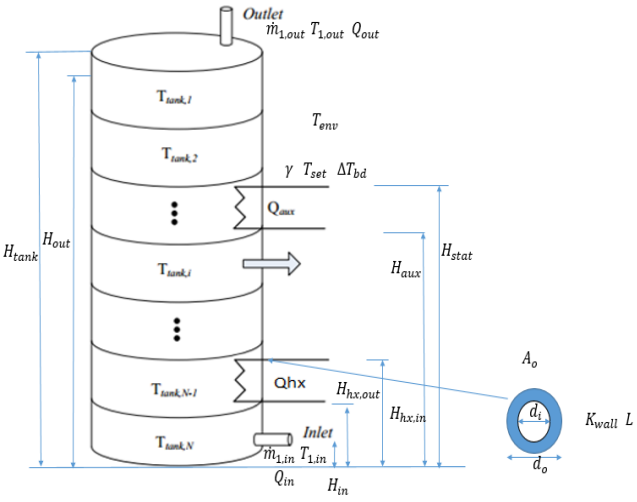

(a) Storage mode

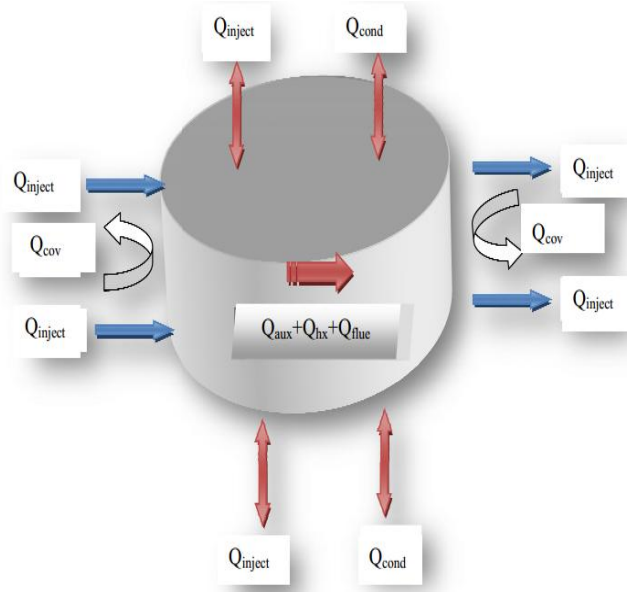

(b) Energy balance conditions on the tank node

Figure 4. Diagram of storage tank and key parameters

4.3 Solar pump

Solar hot water systems commonly employ a direct current (DC) pump that can be directly energised by a solar or photovoltaic (PV) module. The parameters pertaining to the solar pump utilised in the TRNSYS model are presented in Table 4. Equation [7] can be utilised to determine the pump's outlet temperature.

$$T_{fs,out} = T_{fs,in} + \frac{Pf}{\dot{m}_{fs} C_{p,fs}} \quad (15)$$

where $T_{fs,in}$ is the inlet temperature, P is the power of the pump, f is the fraction of the pump's power converted into heat energy of the fluid, $\dot{m}_{fs}$ is the mass flow rate, and $C_{p,fs}$ is the specific heat at constant pressure of the fluid. The mass flow rate at the outlet of the pump can be determined as follows [7]:

$$\dot{m}_{fs,out} = \gamma \dot{m}_{rated} \quad (16)$$

where $\dot{m}_{rated}$ is the nominal mass flow rate, and γ is the control signal of the pump. A linear relationship between flow and energy consumption is assumed as follows [7]:

$$P = \gamma\, P_{rated} \quad (17)$$

Where P_{rated} is the nominal power of the pump in kj/hr.

Table 4. Characteristics of the single-speed pump (Type 3b) [41].

Variable	Value
Flow rate under standard conditions (kg hr^{-1})	212.0
Fluid's specific heat capacity (KJ Kg^{-1} K^{-1})	3.708
Power rating under specified conditions (KJ hr^{-1})	226.8

4.4 Differential temperature controller

The differential temperature controller (DTC) is an electronic device that compares the temperatures of two locations using electronic sensors. It contains a logic component that can turn on or off a relay at appropriate times and a built-in microprocessor that can activate one or more pumps when the temperature is warmer at one location than at another. This device includes a relay switch that controls the pump operation [42].

To generate a control function γ_0 [0 or 1], the DTC considers the upper and lower input temperatures (T_H and T_L, respectively) and the upper and lower dead band temperature differences (ΔT_L and ΔT_L). The new value of γ_0 depends on the input control function γ_i [0 or 1] [7].

If the temperature at the monitored location (T_{IN}) exceeds the high limit condition ($T_{high\ limit}$), the control function will be set to zero, assuming the DTC was previously operational:

$$If\ \gamma_i = 1\ and\ \Delta T_L \le (T_H - T_L)\ ,\ \gamma_0 = 1 \quad (18)$$

$$If\ \gamma_i = 1\ and\ \Delta T_L > (T_H - T_L)\ ,\ \gamma_0 = 0 \quad (19)$$

If the controller was previously off:

$$If\ \gamma_i = 0\ and\ \Delta T_H \le (T_H - T_L)\ ,\ \gamma_0 = 1 \quad (20)$$

$$If\ \gamma_i = 0\ and\ \Delta T_H > (T_H - T_L)\ ,\ \gamma_0 = 0 \quad (21)$$

4.5 Water supply profile (TRNSYS Type 14e)

In order to effectively simulate a hot water system, the hot water load profile is needed, which delineates the temporal consumption of hot water, note, however, that in certain instances, a daily circulation profile is employed without any alterations to depict varying usage patterns during weekends or seasonal fluctuations, as shown in Figure 5.

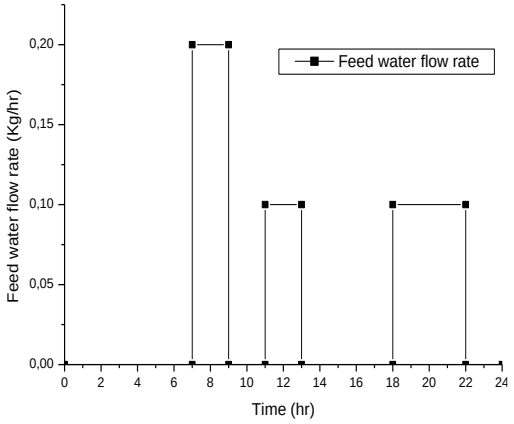

Figure 5. Water supply profile

4.6 Weather data reading and processing (TRNSYS TYPE15-6TM2)

The weather data utilised for the models in this work was acquired from typical weather year (TMY) files, employing TYPE 109-TMY2 to extract hourly weather data. The Metronome files for Ain Témouchent, Algeria, were specifically used.

4.7 DC/AC converter

Two energy conditioning devices, specifically a regulator and an inverter, are necessary components for photovoltaic power systems. The regulator's role is to distribute the direct current generated by the solar cell group to the battery. The inverter is responsible for converting the DC power into AC power and directing it towards the load or, in the case of a fully charged battery, back to the grid. In situations when there is excess energy, it is discharged. [7].

4.8 Battery

The lead-acid battery model is a significant component in a solar power system, encompassing solar cells and power conditioning elements. The battery's state of charge is characterised by its variation over time, which is contingent upon the pace at which it is charged or discharged. The advanced modes of the model additionally encompass formulas pertaining to battery voltage, current, and state of charge [7]. The Shepherd equations, which use power as input, correspond to TYPE47c:

Discharge voltage (I <0):

$$V = e_{qd} - g_d H + I r_{qd}\left(1 + \frac{m_d H}{\frac{Q_d}{Q_m} - H}\right) \quad (22)$$

Charge voltage (I> 0):

$$V = e_{qc} - g_c H + I r_{qc}\left(1 + \frac{m_c H}{\frac{Q_c}{Q_m} - H}\right) \quad (23)$$

The open circuit voltages at full charge and extrapolated from V vs I curves on charge and discharge are represented by e_{qc} and e_{qd}, respectively. The

coefficients of H in voltage-current-state of charge formulas are represented by g_c and g_d, which have small values. The internal resistances at full charge when charging and discharging are represented by r_{qc} and r_{qd}, respectively. The parameters m_c and m_d are used to determine the shapes of the I-V-Q characteristics specific to each cell type. The capacity parameters for charge and discharge are represented by Q_c and Q_d, respectively, while Q_m represents the rated capacity of the cell.

4.9 DCMD module

In order to conduct the simulation with TRNSYS17 software, an additional component, namely TYPE 223, was incorporated into the standard library. This component has been specifically developed to cater to the requirements of a desalination unit employing the DCMD process. The abovementioned component is implemented using the FORTRAN programming language and encompasses a range of parameter values for the DCMD model, as illustrated in the provided reference [6].

5. Results and Discussion

In order to verify the accuracy of our simulation utilising the recently developed TRNSYS component for the DCMD unit, an investigation was carried out on the system devised by Zhang et al. [37], encompassing a diverse set of velocities and temperatures. The experimental data was compared to the data generated by the suggested model, utilising optimal parameters [34]. The comparison was conducted for co-current setups, with a flow speed of 0.4 m/s and constant inlet temperatures of 60 °C and 20 °C for the feed and permeate, respectively. Perspex modules with varying membrane lengths were employed for this analysis. The prior research findings [6, 42] suggest that the current model accurately predicts the permeate flux, as it aligns well with experimental data. On average, there is an 8% discrepancy for a length of 0.07 m. The flux exhibits a gradual and consistent reduction in the flow direction, while the permeation flux demonstrates an increase as the circulation velocity of the feed fluid rises. Moreover, the permeate flux exhibits an increase as the feed temperature rises, owing to the reliance of the partial vapour pressure at the membrane surface on the feed temperature, as described by the Antoine equation. Figure 6 illustrates the discrepancy between the current modelling and experimental findings [37], spanning a range of 0.27 % to 17 %. The observed rise in inaccuracy can be attributed to the utilisation of adjustment equations within the modelling process [6, 42].

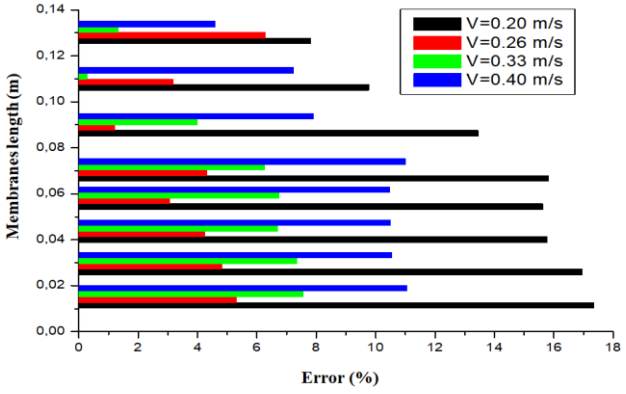

Figure 6. The error between the present modelling and experiment shown in Zhang et al. [37] for different feed fluid velocities.

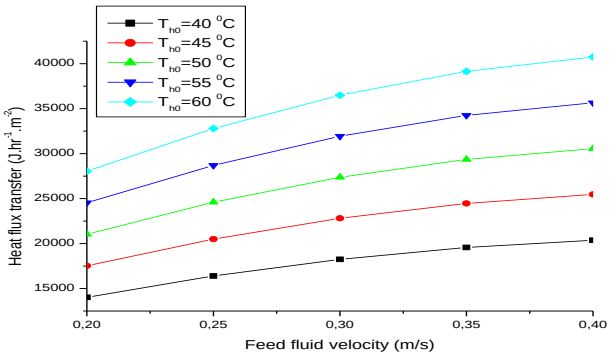

Figure 7. The effect of the feed fluid velocity on heat flux transfer for several hot fluid temperatures.

The correlations between heat flux transfer and feed velocity are shown in Figure 7, where a positive correlation is observed between flow velocity and heat transfer across the membrane, as supported by earlier studies [6, 42]. Moreover, the thermal energy transfer across the membrane is enhanced when the feed water temperature increases while maintaining a constant cooling water temperature of 20°C. The maximum heat transfer through the membrane recorded was 40.74 kJ.hr^{-1}.m^{-2}.

5.1 Meteorological data

In order to simulate the system's behaviour during the specific month of June and forecast its performance, the researchers employed a Typical Meteorological Year (TMY) dataset for Ain Témouchent. Figure 8 displays the annual solar radiation variations, ambient temperature, and wind speed. During the exceptionally hot day, the recorded solar radiation reached an estimated value of 2966 kJ/h m^2. Furthermore, it is worth noting that the most elevated documented ambient temperature reached 30°C, while the utmost recorded wind speed amounted to 10 m/s.

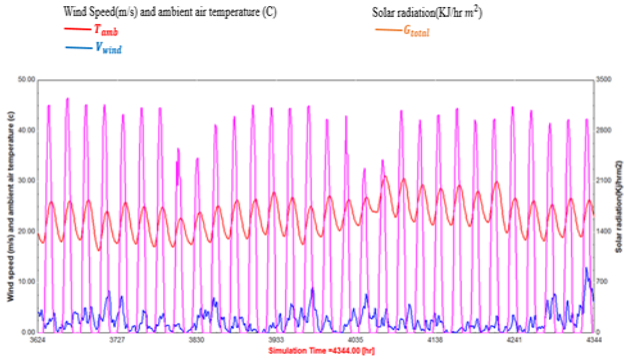

Figure 8. Variations in weather data of Ain Témouchent in the left axes wind speed and ambient air temperature and right axes solar radiation over June

5.2 Thermal system results

Figure 9 illustrates the thermal performance fluctuations of the PVT collector. The left vertical axis indicates the temperatures at the entrance and outflow. In contrast, the right vertical axis shows the flow rate of the solar fluid and the quantity of usable thermal energy generated over June. The results obtained from the simulation indicate that the initial temperature of the PVT collector constantly remains within the interval of 20°C to 60°C, whereas the final temperature ranges from 20°C to 85°C.

Moreover, the simulation results illustrate a range of useable thermal energy, with a peak value of 4000 kJ/h, attributable to the high efficiency attained by the absorption of lead from the solar panels. The curve on the shared axis illustrates the fluctuations in the total flow rate of the solar fluid

circulating within the enclosed system. The pump facilitates the flow rate and has the potential to reach a maximum value of 212 kg/h. Figure 10 depicts the temperature levels of the fluid measured at the top, middle, and bottom of the storage tank for the PVT system during June. The peaks show varying temperature levels between 56°C and 60°C, 32°C and 60°C, and 20°C and 58°C, respectively. These temperature variations result from ambient temperature changes and the tank's specific area in which the liquid temperature was measured.

In addition, it is observed that the storage tank experiences a minor fluctuation in the highest temperature of the fluid. This variation is attributed to the use of auxiliary heating, which can raise the temperature to a maximum of 60°C. Moreover, the heating element exhibits a dead band of 5°C.

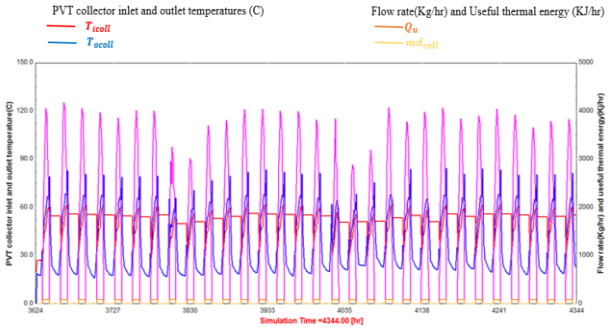

Figure 9. Variations in the thermal system result in left axes PVT collector inlet and outlet temperatures and in the right axes solar fluid flow rate and valuable thermal energy over June

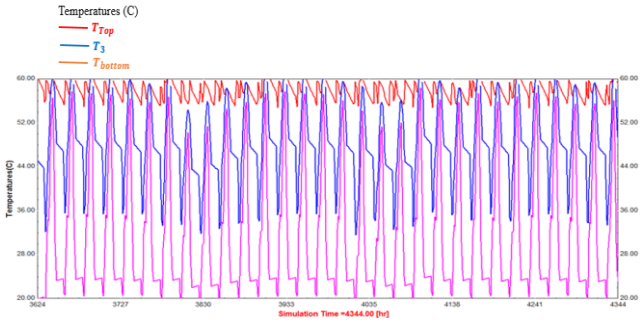

Figure 10. Variations of temperature levels of the fluid at the top, middle and bottom of the storage tank over June.

Figure 11 illustrates the auxiliary heating rate and energy input from the heat exchanger on the left axis and the storage tank's intake and outflow flow rates throughout June on the right axis. The modelling results indicate that the energy provided by the auxiliary heater (Q_{aux}) attains its maximum value of 10 10^3 kJ/hr. Furthermore, the heat exchanger located within the storage tank facilitates energy transmission from the solar fluid to the salt water, resulting in a rate of 5000 KJ/hr.

Additionally, the modelling results demonstrate that the seawater mass flow rate entering and exiting the storage tank attains a maximum value of 20 Kg/hr for both. The solar fraction (SF) concept is used to explain the system's performance. SF is defined as the ratio of the thermal energy used to heat seawater provided by the heat exchanger (Qhx) to the total energy, which includes both the thermal energy and electrical energy required (Qaux). It can be calculated as follows [40,41]:

$$SF=Q_{hx}/(Q_{aux}+Q_{hx}) \quad (24)$$

Figure 12 clarifies changes in solar fraction (SF), this is due to the fluctuation of solar radiation, which leads to a change in the energy absorbed by PVT collectors and, of course, a change in the energy provided by the heat exchanger to seawater. SF varies from 15 % to 30 %.

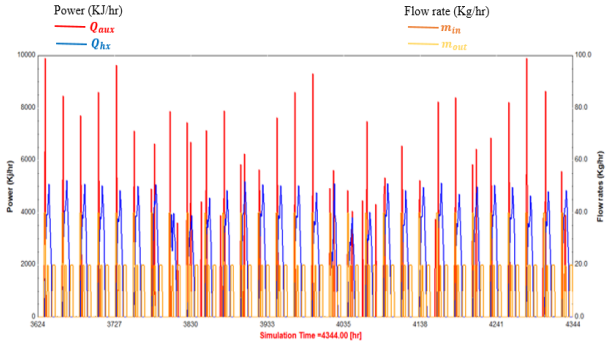

Figure 11. Variations of auxiliary heating rate, energy input from the heat exchanger, and storage tank's inlet and outlet flow rates over June.

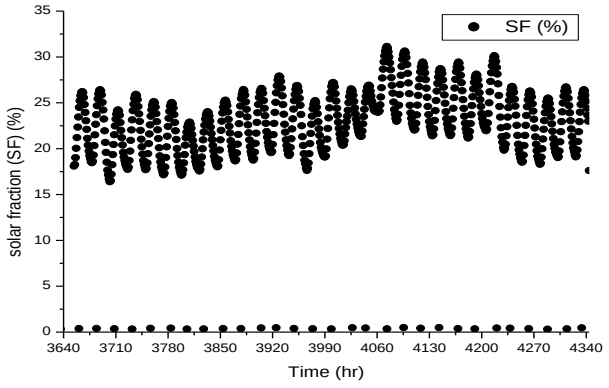

Figure 12. A solar fraction over Jun

5.3 PV system results

Figure 13 illustrates the fluctuations in the power equilibrium of the inverter, the power derived from the solar photovoltaic (PV) array (incoming power from generation), and the power consumed by the load throughout the designated month of testing (June). The findings indicate that the photovoltaic (PV) array achieved its maximum power output at 2.5 kW, but the load required 2.4 kW. The energy necessary for heating water is derived from a combination of thermal energy and supplementary heating, as shown in Figure 12. The heat exchanger delivered an estimated energy output of roughly 1.3 kilowatts, whereas the auxiliary heater provided an energy input of 2 kW, as depicted in Figure 11. The Type 48b (Regulator/Inverter) was employed to provide the requisite supplementary electrical power.

In order to have a more detailed understanding of the power output of the photovoltaic (PV) array, two specific days were chosen for analysis, as illustrated in Figure 14. The monthly average power generation of the photovoltaic (PV) array in June ranges from 169 W to 134 W.

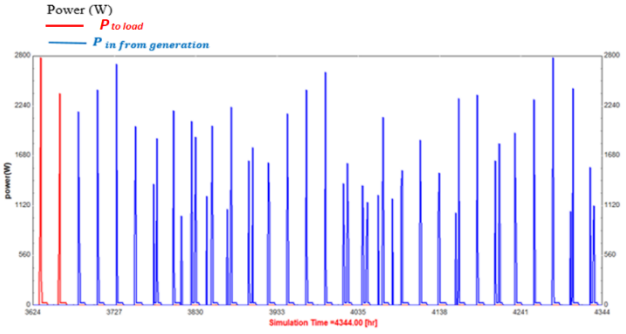

Figure 13. Variations of power in from generation and power to load over June.

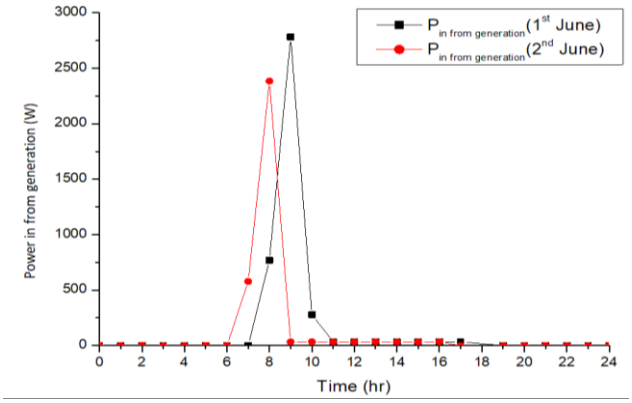

Figure 14. Variations of power in from generation on 1st and 2nd June.

Figure 15 illustrates the fluctuations in photovoltaic efficiency observed on 21 June. The graph represents a progressive improvement in efficiency from 8 am to 6 pm, culminating in a value of 0.66. The observed rise can be attributed to variations in solar radiation. Nevertheless, the image does not exhibit any discernible effects of decreasing temperatures on the efficiency of photovoltaic (PV) systems. It is noted that elevated cooling temperatures of a photovoltaic-thermal (PVT) collector might exert a detrimental impact on its overall efficiency.

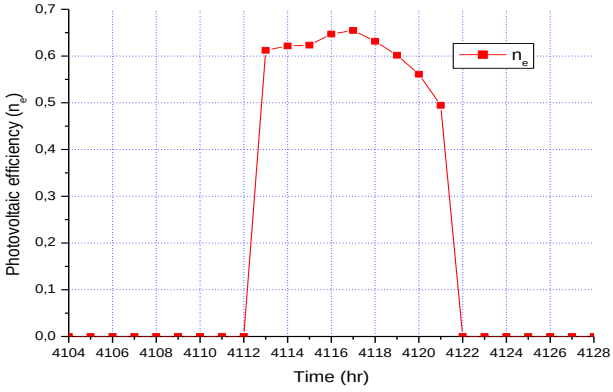

Figure 15. Variations of photovoltaic efficiency on 21 June.

5.4 DCMD module results

Figure 16 presents the fluctuation of permeate flux. The maximum distillate output per membrane area is 12 L/m^2.hr. The variability in productivity can be ascribed to diurnal fluctuations in solar radiation, which subsequently impact the temperature of the feed water and, consequently, the rate of permeate flux. Furthermore, it is noted that the distribution of the feed mass flow rate exhibits variations throughout the course of the day, which in turn contributes to the observed fluctuations in productivity. The mean monthly permeate flux was determined to be 5.556 L/m^2.hr.

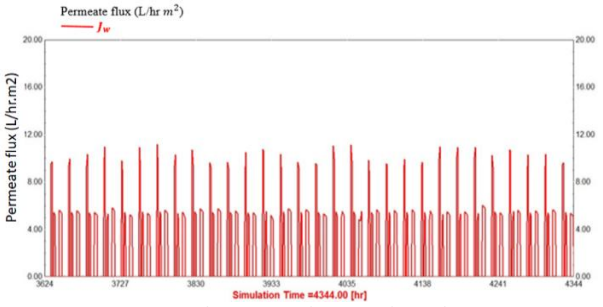

Figure 16. Variations of total mass flux transfer J_w for DCMD system over Jun.

Figure 17 illustrates the fluctuations in the temperatures of the feed and permeates (Thout and Tcout) as they exit the DCMD system throughout June. The observed drop in the exit temperature of the feed is in line with the findings described earlier. Also, it is seen that the temperature of the permeate water outlet rises throughout the course of the day, suggesting a rise in heat transmission.

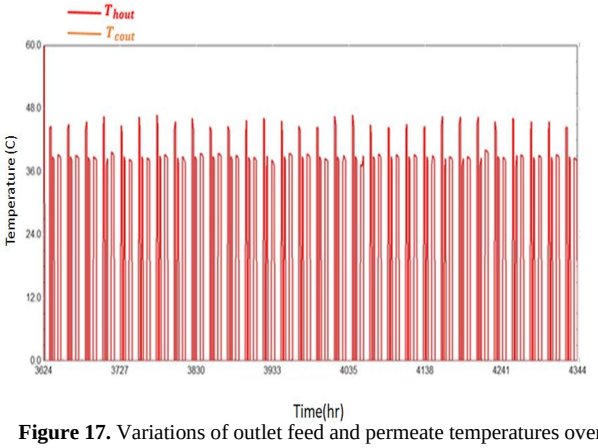

Figure 17. Variations of outlet feed and permeate temperatures over June.

To clearly depict the variations in outlet feed and permeate temperatures, as well as permeate flux, throughout the course of a day, the date of 21 June was chosen, as illustrated in Figure 18. In the co-current flow setup, it is seen that the feed temperature experiences a decline while the distillate temperature exhibits an increase during the course of the day. The permeate flux gradually rises during the day, displaying an average daily magnitude of 6.22 L/m^2 day.

Table 5 provides a comparison between the current study and previous studies on (PVT+MD) or (PV+thermal collector+MD) systems to confirm the usability of PVT collectors in salt-water desalination systems with MD. The results show that the present system produced 12 L/m^{2}h of potable water using PVT, which is higher than the systems developed using CPVT [27,28,30,42] or mixed two desalination technologies [42].

This finding provides evidence supporting the viability of the existing system in terms of generating drinkable water. In order to enhance productivity and address deficiencies in the process, it is recommended to exercise control over stratification through the implementation of hot water outlets positioned at the location of the heat exchanger or the use of supplementary storage facilities external to the tank. The inclusion of supplementary storage within the tank has the potential to disrupt stratification, hence impacting the supply of cooling water to the PVTs.

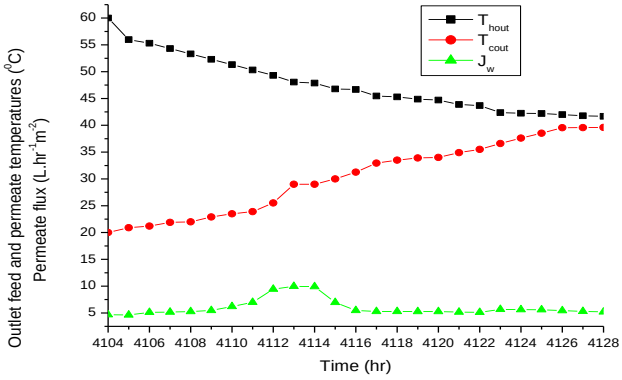

Figure 18. Variations of outlet feed and permeate temperatures and permeate flux on 21 June.

Table 5. Comparison between present study and previous studies in (PVT+MD) or (PV+ thermal collector +MD) systems for seawater desalination.

System	Collector Area	Generating drinkable water	Reference
Present system (PVT+DCMD)	2 m^2 of PVT area	12 L/m^2h	-
CPVT+AGMD	1 m^2 of CPVT aperture area	3.4 L/m^2h	[27,28]
CPVT+DCMD	-	7.1 L/m^2h	[28,30]
(PV+FPC)+DCMD	2 m^2 of FPC absorber area	11.09 L/m^2h	[42]

6. CONCLUSIONS

The operational effectiveness of a solar-powered desalination system that incorporates photovoltaic thermal (PVT) collectors and a direct contact membrane distillation (DCMD) module is assessed. Dynamic simulations were conducted using TRNSYS software to simulate real-world climatic conditions in Ain Témouchent, Algeria. The research incorporated and simulated a novel DCMD module for seawater desalination. Additionally, parametric analyses were performed to examine several factors like the feed water mass flow rate and hot feed temperature. The study's findings indicated a positive correlation between the inlet feed temperature and the permeate flux. Specifically, when the inlet feed temperature was raised from 40°C to 80°C, the permeate flux exhibited an increase ranging from 10 to 80 L/h.m^2. Additionally, it was observed that raising the circulating velocity of the feed fluid from 0.20 m/s to 0.40 m/s while maintaining a constant feed inlet temperature also resulted in an increase in permeate flux. Regarding the PVT-DCMD system, the outlet temperature of the PVT collector fluctuated between 20 °C to 85 °C, and the fluid temperatures at the top, middle, and bottom of the storage tank of the PVT system varied between 56 °C to 60 °C, 32 °C to 60 °C, and 20 °C to 58 °C, respectively, throughout June. The heat exchanger yielded an energy output of roughly 1.3 kW, while the auxiliary heater contributed an additional 2 kW of energy. Moreover, the feed outlet temperature of the DCMD system experienced a decline due to variations in solar radiation during the day. Conversely, the permeate water outlet temperature exhibited an increase due to enhanced heat transfer. Future work appears to be merited on strategies for the reuse of concentrated water or the retrieval of lost heat, with the aim of improving the production of distillate. The distillate production achieved a peak value of 12 L/h per membrane area while maintaining an average monthly value of 5.556 L/m^2 in the month of June. In addition, the photovoltaic (PV) efficiency was determined to be 0.66, which was adversely affected by the elevated cooling temperatures associated with the PVT collector. Hence, additional investigations are needed on the cooling temperature of the PVT collector, as is a comprehensive technical and economic analysis, to substantiate this system's practical and financial viability.

Authors' contribution

All authors contributed equally to the preparation of this article.

Declaration of competing interest

The authors affirm that they do not have any known financial or personal relationships that could have affected the impartiality of the work presented in this paper.

Funding source

This study didn't receive any specific funds.

Data availability

The data that support the findings of this study are available from the corresponding author upon reasonable request.

REFERENCES

[1] Hezam, AL-AImmari, Nabil Abdullah Noman Alkadasi, and Abdul Jabar Mohammed Saleh AL-Eyani. "Take advantage of the misdirected condensers heat for Mokha steam station to desalinate water for the city of Taiz." Al-Qadisiyah Journal for Engineering Sciences 8.4 (2015): 0-0. https://doi.org/10.60160/1973-000-007-013

[2] Niu, R., Du, J., & Kong, X. "Simulation study of membrane distillation regenerator based on reduced pressure air gap", Journal of Building Engineering, 62 (2022): 105273. https://doi.org/10.1016/j.jobe.2022.105273

[3] Jiwad, Foad Srhan, Mojtaba Behnam Taghadosi, and Ahmed Abed Al-Kadhem Majhool. "Development of the Hydro Static Wind Turbine Powered RO System for Maximum Power Point and Maximum Permeate Flow Tracking." Al-Qadisiyah J Eng Sci 13.1 (2020): 60-6. https://doi.org/10.30772/qjes.v13i1.649

[4] Boukhriss, M., Timoumi, M., & Bacha, H. B., "Experimental of membrane distillation unit coupled with a DCMD using solar energy". Solar Compass, 7(2023): 100055. https://doi.org/10.1016/j.solcom.2023.100055

[5] Lawal, D. U., "Performance enhancement of permeate gap membrane distillation system augmented with impeller". Sustainable Energy Technologies and Assessments, 54 (2022):102792. https://doi.org/10.1016/j.seta.2022.102792

[6] Remlaoui, Ahmed, Driss Nehari, Abderrahmane Elmeriah, and Mohammed Laissaoui. "A TRNSYS model of a direct contact membrane distillation (DCMD) system coupled to a flat plate solar collector (FPC)." J. Eur. des Systèmes Autom. 50 (2017): 335-360. https://doi.org/10.3166/jesa.50.335-360

[7] TRNSYS: Transient System Simulation tool. Available online: http://www.trnsys.com

[8] Kumar, Nutakki Tirumala Uday, and Andrew R. Martin. "Co-production performance evaluation of a novel solar combi system for simultaneous pure water and hot water supply in urban households of UAE." Energies 10, no. 4 (2017): 481. https://doi.org/10.3390/en10040481

[9] Mohan, Gowtham, Uday Kumar, Manoj Kumar Pokhrel, and Andrew Martin. "A novel solar thermal polygeneration system for sustainable production of cooling, clean water and domestic hot water in United Arab Emirates: Dynamic simulation and economic evaluation." Applied energy 167 (2016): 173-188. https://doi.org/10.1016/j.apenergy.2015.10.116

[10] Chafidz, Achmad, Saeed Al-Zahrani, Mansour N. Al-Otaibi, Choo F. Hoong, Tan F. Lai, and Manoharan Prabu. "Portable and integrated solar-driven desalination system using membrane distillation for arid remote areas in Saudi Arabia." Desalination 345 (2014): 36-49. https://doi.org/10.1016/j.desal.2014.04.017

[11] Khordehgah, Navid, Valentin Guichet, Stephen P. Lester, and Hussam Jouhara. "Computational study and experimental validation of a solar photovoltaics and thermal technology." Renewable Energy 143 (2019): 1348-1356. https://doi.org/10.1016/j.renene.2019.05.108

[12] Majeed, Mohammed Abd Al-salam, and Salah M. Salih. "Experimental and theoretical analysis of photovoltaic thermal collector performance

with multi-flow channel." Al-Qadisiyah Journal for Engineering Sciences (2023)

[13] Chow, Tin Tai. "A review on photovoltaic/thermal hybrid solar technology." Renewable Energy (2018): Vol4 88-119. https://doi.org/10.4324/9781315793245-122

[14] Chow, T. T. "Performance analysis of photovoltaic-thermal collector by explicit dynamic model." Solar Energy 75, no. 2 (2003): 143-152. https://doi.org/10.1016/j.solener.2003.07.001

[15] Assoa, Y. B., and C. Ménézo. "Dynamic study of a new concept of photovoltaic–thermal hybrid collector." Solar energy 107 (2014): 637-652. https://doi.org/10.1016/j.solener.2014.05.035

[16] Guarracino, Ilaria, James Freeman, Alba Ramos, Soteris A. Kalogirou, Nicholas J. Ekins-Daukes, and Christos N. Markides. "Systematic testing of hybrid PV-thermal (PVT) solar collectors in steady-state and dynamic outdoor conditions." Applied energy 240 (2019): 1014-1030. https://doi.org/10.1016/j.apenergy.2018.12.049

[17] Guarracino, Ilaria, Alexander Mellor, Nicholas J. Ekins-Daukes, and Christos N. Markides. "Dynamic coupled thermal-and-electrical modelling of sheet-and-tube hybrid photovoltaic/thermal (PVT) collectors." Applied Thermal Engineering 101 (2016): 778-795. https://doi.org/10.1016/j.applthermaleng.2016.02.056

[18] Amrizal, N., D. Chemisana, and J. I. Rosell. "Hybrid photovoltaic–thermal solar collectors dynamic modeling." Applied energy 101 (2013): 797-807. https://doi.org/10.1016/j.apenergy.2012.08.020

[19] Haurant, Pierrick, Christophe Ménézo, Leon Gaillard, and Patrick Dupeyrat. "A numerical model of a solar domestic hot water system integrating hybrid photovoltaic/thermal collectors." Energy Procedia 78 (2015): 1991-1997. https://doi.org/10.1016/j.egypro.2015.11.391

[20] Chen, J. F., L. Zhang, and Y. J. Dai. "Performance analysis and multi-objective optimisation of a hybrid photovoltaic/thermal collector for domestic hot water application." Energy 143 (2018): 500-516. https://doi.org/10.1016/j.energy.2017.10.143

[21] Pierrick, Haurant, Ménézo Christophe, Gaillard Leon, and Dupeyrat Patrick. "Dynamic numerical model of a high efficiency PV–T collector integrated into a domestic hot water system." Solar Energy 111 (2015): 68-81. https://doi.org/10.1016/j.solener.2014.10.031

[22] Thinsurat, Kamon, Huashan Bao, Zhiwei Ma, and Anthony P. Roskilly. "Performance study of solar photovoltaic-thermal collector for domestic hot water use and thermochemical sorption seasonal storage." Energy Conversion and Management 180 (2019): 1068-1084. https://doi.org/10.1016/j.enconman.2018.11.049

[23] Dupeyrat, Patrick, Christophe Ménézo, and S. Fortuin. "Study of the thermal and electrical performances of PVT solar hot water system." Energy and Buildings 68 (2014): 751-755. https://doi.org/10.1016/j.enbuild.2012.09.032

[24] Buonomano, Annamaria, Francesco Calise, and Adolfo Palombo. "Solar heating and cooling systems by absorption and adsorption chillers driven by stationary and concentrating photovoltaic/thermal solar collectors: Modelling and simulation." Renewable and Sustainable Energy Reviews 82 (2018): 1874-1908. https://doi.org/10.1016/j.rser.2017.10.059

[25] Calise, Francesco, Massimo Dentice d'Accadia, and Laura Vanoli. "Design and dynamic simulation of a novel solar trigeneration system based on hybrid photovoltaic/thermal collectors (PVT)." Energy conversion and management 60 (2012): 214-225. https://doi.org/10.1016/j.enconman.2012.01.025

[26] Acevedo, Luis, Javier Uche, Alejandro Del Almo, Fernando Círez, Sergio Usón, Amaya Martínez, and Isabel Guedea. "Dynamic simulation of a trigeneration scheme for domestic purposes based on hybrid techniques." Energies 9, no. 12 (2016): 1013. https://doi.org/10.3390/en9121013

[27] Hughes, A. J., T. S. O'Donovan, and T. K. Mallick. "Experimental evaluation of a membrane distillation system for integration with concentrated photovoltaic/thermal (CPV/T) energy." Energy Procedia 54 (2014): 725-733. https://doi.org/10.1016/j.egypro.2014.07.313

[28] Giwa, Adewale, Ahmed Yusuf, Abdallah Dindi, and Hammed Abiodun Balogun. "Polygeneration in desalination by photovoltaic thermal systems: A comprehensive review." Renewable and Sustainable Energy Reviews 130 (2020): 109946. https://doi.org/10.1016/j.rser.2020.109946

[29] Davis, Thomas A., and Malynda A. Cappelle. "Photovoltaic-Thermal (PV-T) system for desalination." U.S. Patent 9,278,315, issued 08 March, 2016

[30] Krnac, Andrew, Miguel Araiz, Sohel Rana, Jason Velardo, and Abhijit Date. "Investigation of direct contact membrane distillation coupling with a concentrated photovoltaic solar system." Energy Procedia 160 (2019): 246-252. https://doi.org/10.1016/j.egypro.2019.02.143

[31] Selvi, S. R., and R. Baskaran. "Solar photovoltaic-powered membrane distillation as sustainable clean energy technology in desalination." Current science (2015): 1247-1254. https://doi.org/10.18520/cs/v109/i7/1247-1254

[32] Wiesenfarth, Maike, Joachim Went, Armin Bösch, Alexander Dilger, Thomas Kec, Achim Kroll, Joachim Koschikowski, and A. W. Bett. "CPV-T mirror dish system combined with water desalination systems." In AIP conference proceedings, vol. 1766, no. 1. AIP Publishing, 2016. https://doi.org/10.1063/1.4962076

[33] Li, Guopei, and Lin Lu. "Modeling and performance analysis of a fully solar-powered standalone sweeping gas membrane distillation desalination system for island and coastal households." Energy conversion and management 205 (2020): 112375. https://doi.org/10.1016/j.enconman.2019.112375

[34] Zhang, Zhaoli, Zicheng Hu, Huibin Xu, Xiaoli Dai, Junfeng Wang, Wenrui Jiao, Yanping Yuan, and Patrick Phelan. "Theoretical analysis of a solar-powered multi-effect distillation integrated with concentrating photovoltaic/thermal system." Desalination 468 (2019): 114074. https://doi.org/10.1016/j.desal.2019.114074

[35] Abdelgaied, Mohamed, Mohamed Fathi Seleem, Mohamed Mahgoub Bassuoni, and Ahmed M. Khaira. "Performance of a solar hybrid desalination plant integrated with photovoltaic-thermal collectors for remote regions: Experimental and modeling investigation." Solar Energy 264 (2023): 112082. https://doi.org/10.1016/j.solener.2023.112082

[36] Chen, Qian, Muhammad Burhan, Faheem Hassan Akhtar, Doskhan Ybyraiymkul, Muhammad Wakil Shahzad, Yong Li, and Kim Choon Ng. "A decentralised water/electricity cogeneration system integrating concentrated photovoltaic/thermal collectors and vacuum multi-effect membrane distillation." Energy 230 (2021): 120852. https://doi.org/10.1016/j.energy.2021.120852

[37] Zhang, Jianhua, Jun-de Li, and Stephen Gray. "Researching and modelling the dependence of MD flux on membrane dimension for scale-up purpose." Desalination and Water Treatment 31, no. 1-3 (2011): 144-150. https://doi.org/10.5004/dwt.2011.2373

[38] Eleiwi, Fadi, Noreddine Ghaffour, Ahmad S. Alsaadi, Lijo Francis, and Taous Meriem Laleg-Kirati. "Dynamic modeling and experimental validation for direct contact membrane distillation (DCMD) process." Desalination 384 (2016): 1-11. https://doi.org/10.1016/j.desal.2016.01.004

[39] Tiwari, G. N., Md Meraj, M. E. Khan, R. K. Mishra, and Vihang Garg. "Improved Hottel-Whillier-Bliss equation for N-photovoltaic thermal-compound parabolic concentrator (N-PVT-CPC) collector." Solar Energy 166 (2018): 203-212. https://doi.org/10.1016/j.solener.2018.02.058

[40] Ayompe, L. M., Aidan Duffy, S. J. McCormack, and Michael Conlon. "Validated TRNSYS model for forced circulation solar water heating systems with flat plate and heat pipe evacuated tube collectors." Applied Thermal Engineering 31, no. 8-9 (2011): 1536-1542. https://doi.org/10.1016/j.applthermaleng.2011.01.046

[41] Ramlow, Bob, and Benjamin Nusz. Solar water heating: a comprehensive guide to solar water and space heating systems. New Society Publishers, 2010.

[42] Remlaoui, Ahmed, Driss Nehari, Mohammed Laissaoui, and Abdelfatah Marni Sandid. "Performance evaluation of a solar thermal and photovoltaic hybrid system powering a direct contact membrane distillation: TRNSYS simulation." Desalination and Water Treatment 194 (2020) https://doi.org/10.5004/dwt.2020.25834